Electronic Supplementary Material (ESI) for Energy & Environmental Science.

Electronic Supplementary Information

First Turnover Analysis of Water-Oxidation Catalyzed by Co-oxide Nanoparticles

*S. Koroidov[a], M. F. Anderlund[b], S. Styring[b], A. Thapper[b] and J. Messinger[a]**

[a] Department of Chemistry, Kemiskt Biologiskt Centrum (KBC), Umeå University, S-90187 Umeå, Sweden.

[b] Molecular Biomimetics, Department of Chemistry – Ångström Laboratory, Uppsala University, S-75120 Uppsala, Sweden.

Text S1

XPS, XRD and DLS experiments were collected on a slightly modified preparation, since the exact same conditions as in the manuscript are too dilute for obtaining enough solid material to conduct XRD and XPS experiments. For preparation we followed the procedure worked out by Risch et al.. [1] The DLS data show that the nano-particles prepared using this procedure have a 10-times larger diameter than in the MIMS experiments (Fig S1). The XRD data presented in Figure S2 confirm the amorphous nature of the Co/M2P nano-particles. For comparison also the XRD of commercial Co_3O_4 nano particles (Sigma Aldrich) is shown, which clearly shows diffraction peaks. The XPS data (Fig. S3) are consistent with the expected Co/μ-O ratio of 7/12 for Co/M2P fragments containing 7 Co ions. The data also reveal a ratio of 7 Co to 6 P, raising the possibility of the ligation of 3 M2P ligands to the Co_7-fragments. As detailed in the main manuscript, we think that in suspension (as opposed to this solid state material) the M2P is not firmly ligated to Co, but instead mobile. Importantly, Figure S4 shows that also if 3 M2P-ligands would be bound to the Co_7-fragments the proposed mechanism (Figure 7) is viable.

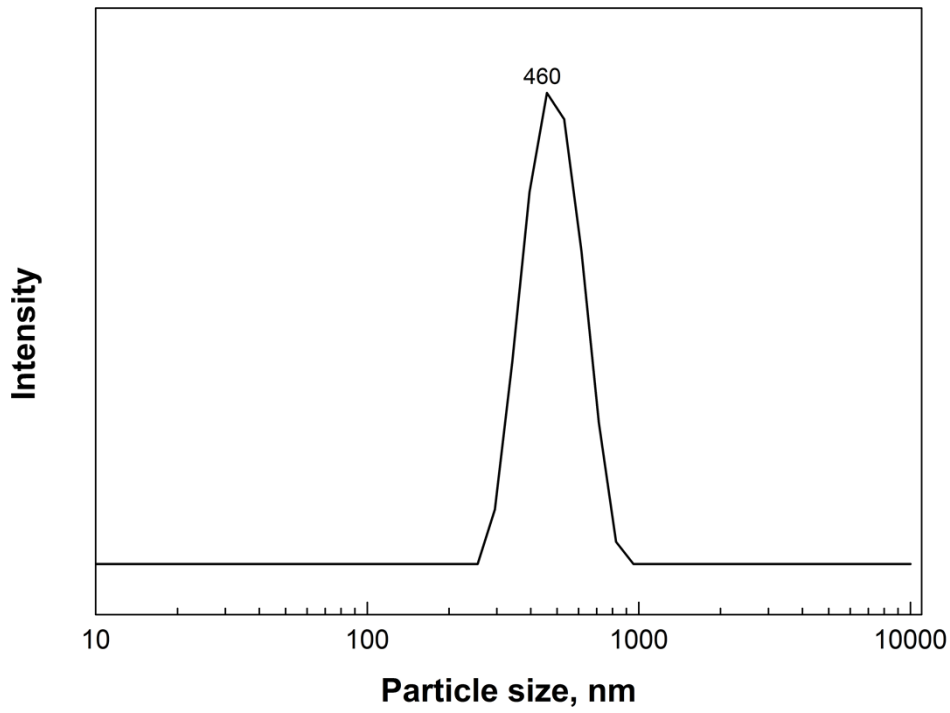

Figure S1. DLS (dynamic light scattering) measurement of Co/M2P NP (1mg/ml) powder suspended in 20 mM P_i buffer (pH 7). The DLS measurement was performed at 25 ^{0}C with a scattering angle of 173^o using a Zetasizer Nano ZS instrument (Malvern Instruments).

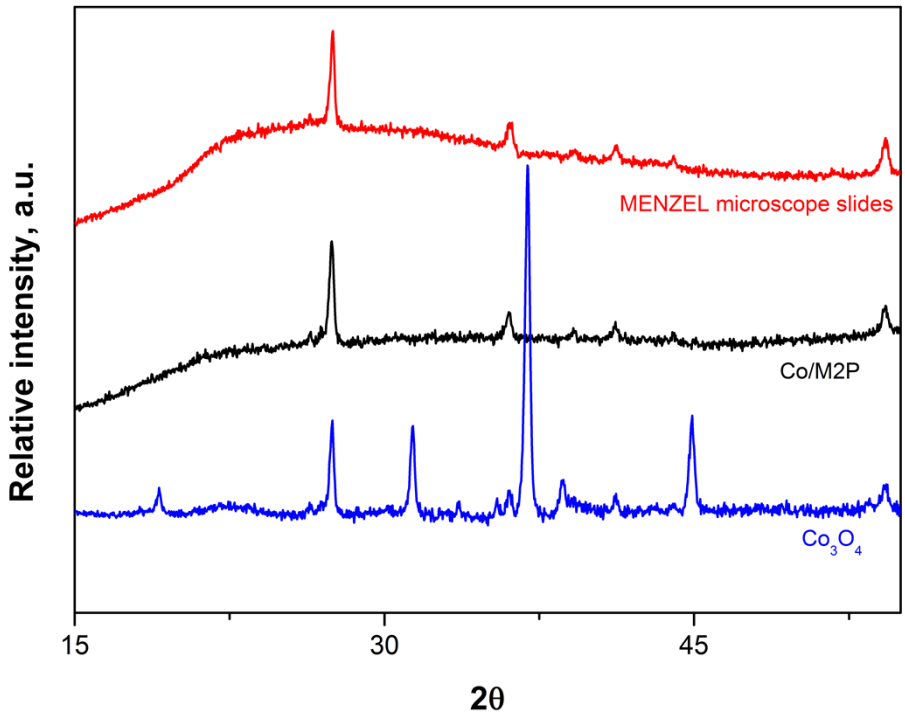

Figure S2. Powder x-ray diffractograms of commercial crystalline Co_3O_4 nano-powder (blue line), of synthesized Co/M2P powder (black) and of the blank MENZEL microscope slides (red), which were used as support for both samples. The diffractograms show that Co/M2P powder is amorphous with no crystalline domains. XRD measurements were performed from 2Θ = 15° to 55° with a step size of 0.03° and 20 sec per step using a Siemens D5000 diffractometer. The diffractometer was operated at an X-ray voltage of 40 kV and an X-ray current of 30 mA.

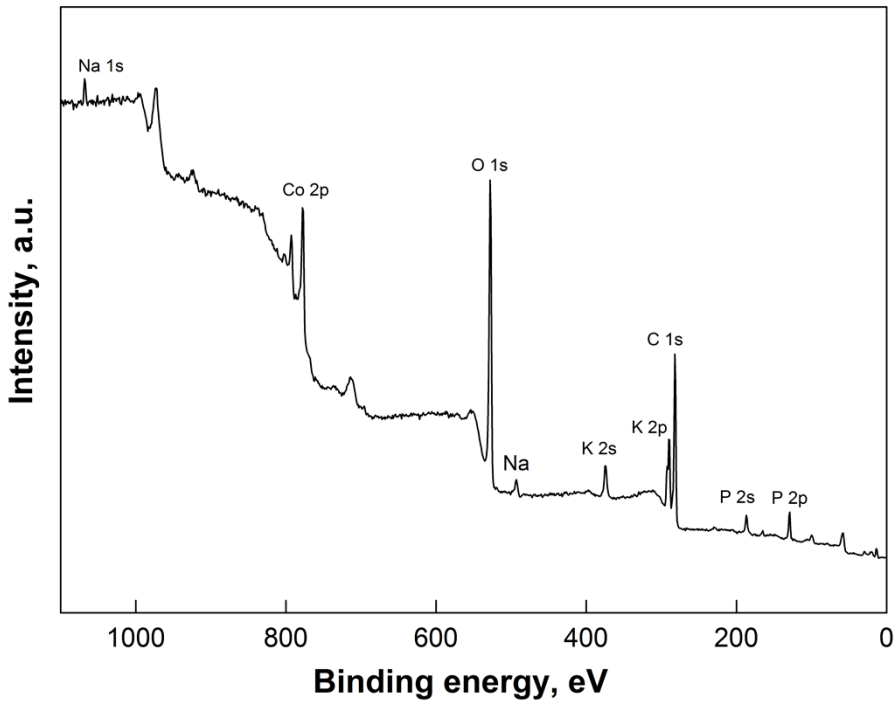

Figure S3. X-ray photoelectron spectroscopy (XPS) spectrum of the synthesized Co/M2P powder. The data were collected using a Kratos Axis Ultra DLD electron spectrometer equipped with a monochromatized Al Kα source operated at 150 W.

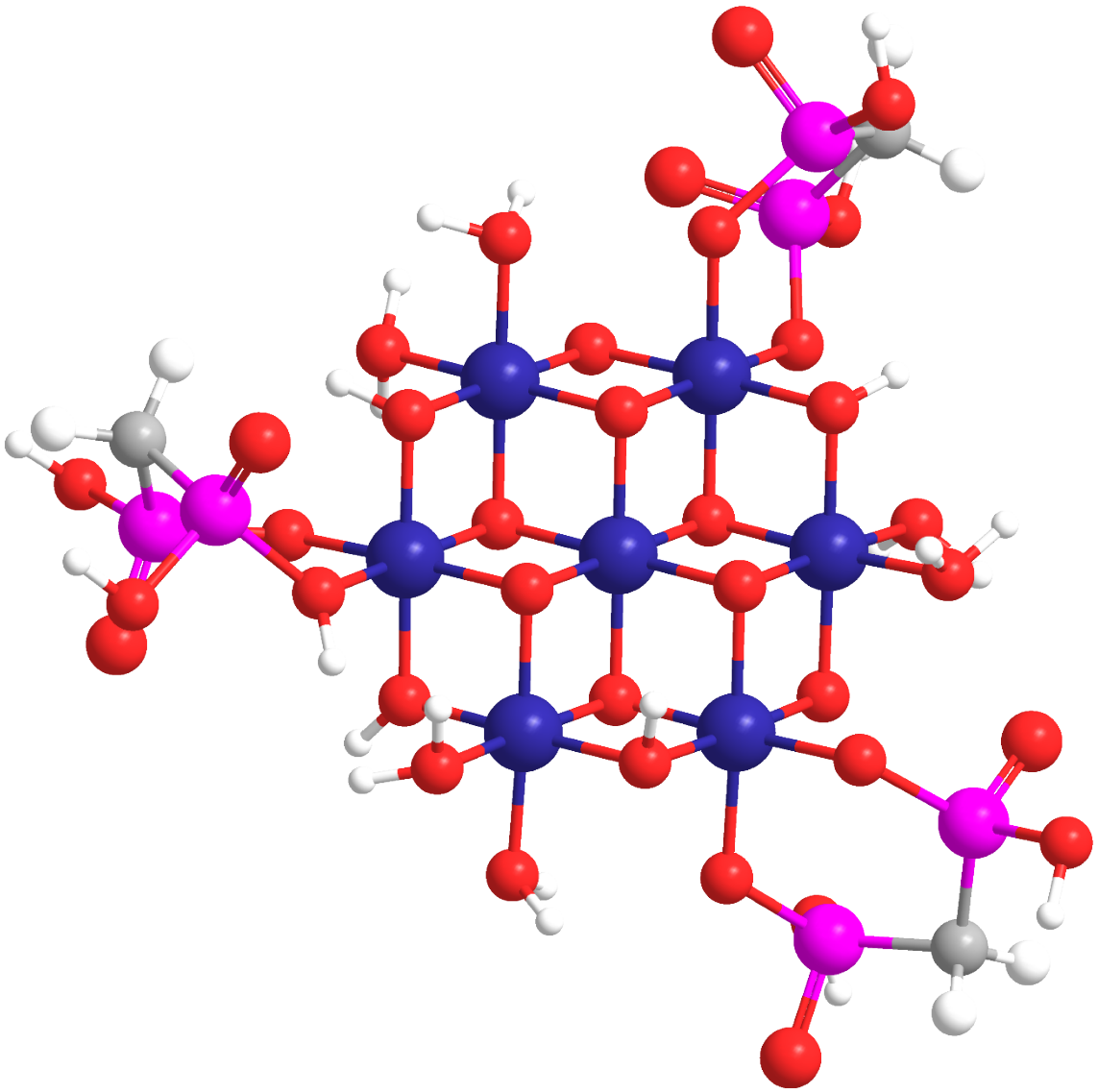

Figure S4. Possible XPS-consistent structural motif for the Co/M2P powder synthesized according to the procedure described by Risch et al.[1]. Alternatively, the M2P ligands may bridge each two neighboring Co-ions, or may intercalate between Co-oxide layers. This possible solid state structure does not necessarily reflect the situation in suspension, where the M2P molecules may be more mobile and all terminal ligands may be water molecules in the resting state (see main text).

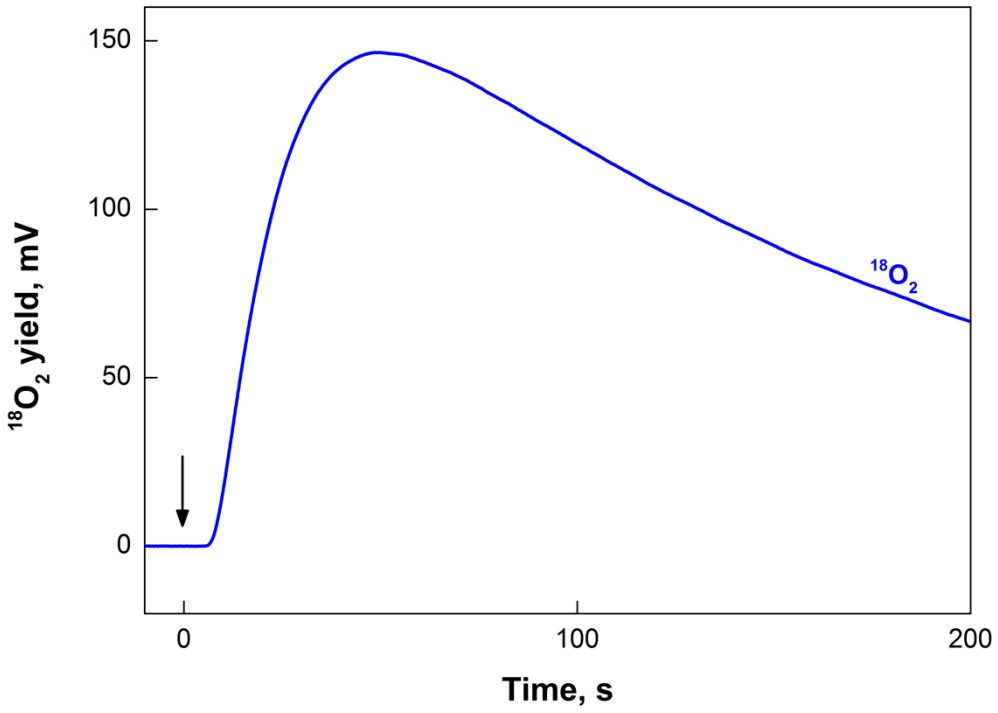

Figure S5. Injection of 100 µl $[Ru(bpy)_3]^{3+}$ dissolved in 90% labeled P_i buffer that was stored for several minutes in a glass syringe (with metal needle) into P_i buffer giving final enrichment of 15% ^{18}O and 76 µM $[Ru(bpy)_3]^{3+}$. The arrows indicate the time of injection. The signal equivalent to 12 nM of $^{18}O_2$ that is formed in the syringe. See also references[2, 3] for earlier descriptions of small O_2 evolution by $[Ru(bpy)_3]^{3+}$ in aqueous P_i solutions.

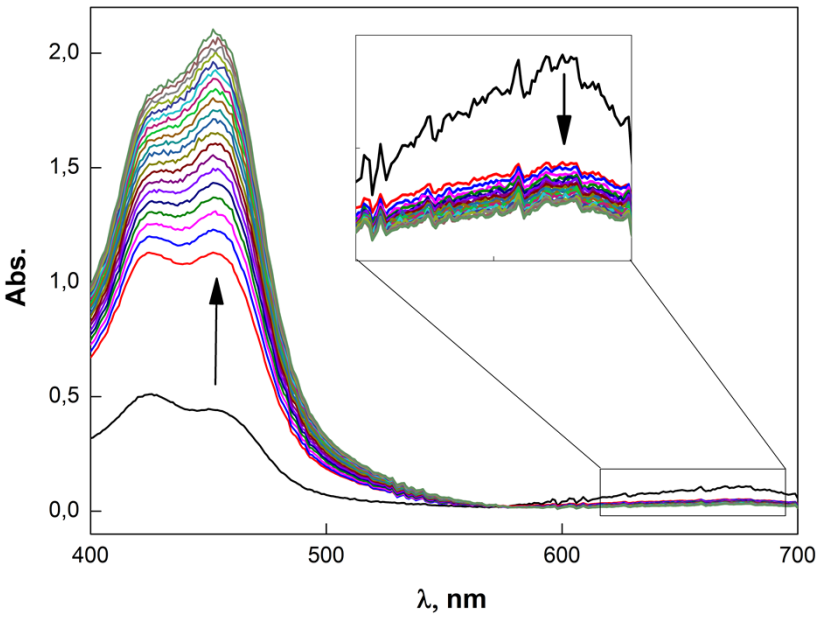

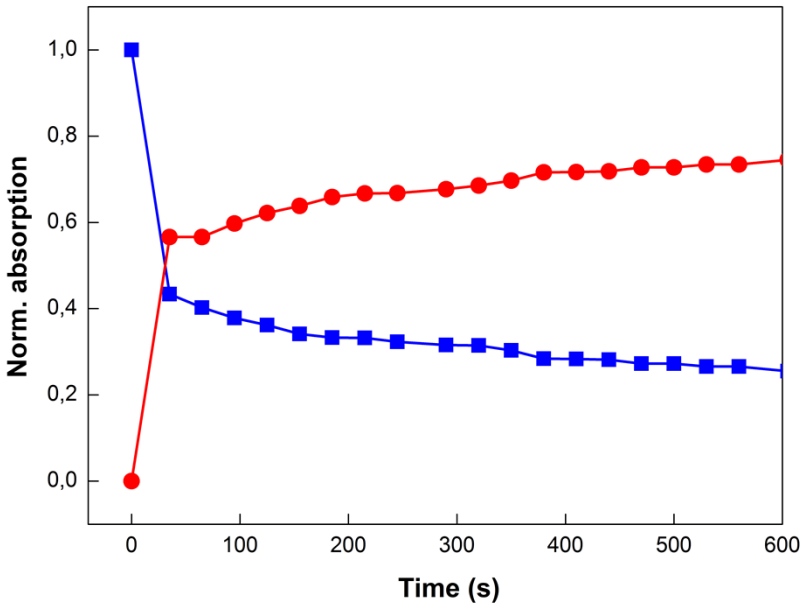

Figure S6, top: Absorbance of a solution of 1 mM $[Ru(bpy)_3]^{3+}$ in in 4 M H_2SO_4 (black line) and the time dependent conversion of 1 mM $[Ru(bpy)_3]^{3+}$ into $[Ru(bpy)_3]^{2+}$ in 20 mM P_i buffer at pH 7.0. **Bottom:** Absorbance-time profiles at λ =454 nm and λ = 675 nm for a solution with initially 1 mM $[Ru(bpy)_3]^{3+}$ in 20 mM P_i buffer at pH 7.0; the two selected wavelength are the absorption maxima of $Ru(bpy)_3]^{2+}$ (red circles) and $[Ru(bpy)_3]^{3+}$ (blue triangles), respectively. The data are normalized to the absorption obtained with a 1 mM $[Ru(bpy)_3]^{3+}$ solution in 4 M H_2SO_4. Zero for $[Ru(bpy)_3]^{2+}$ corresponds for 27 μM. It was demonstrated previously that the lifetime of $[Ru(bpy)_3]^{3+}$ in 4 M H_2SO_4 is 25 h or longer,[2, 4] thus allowing a reliable 100% determination.

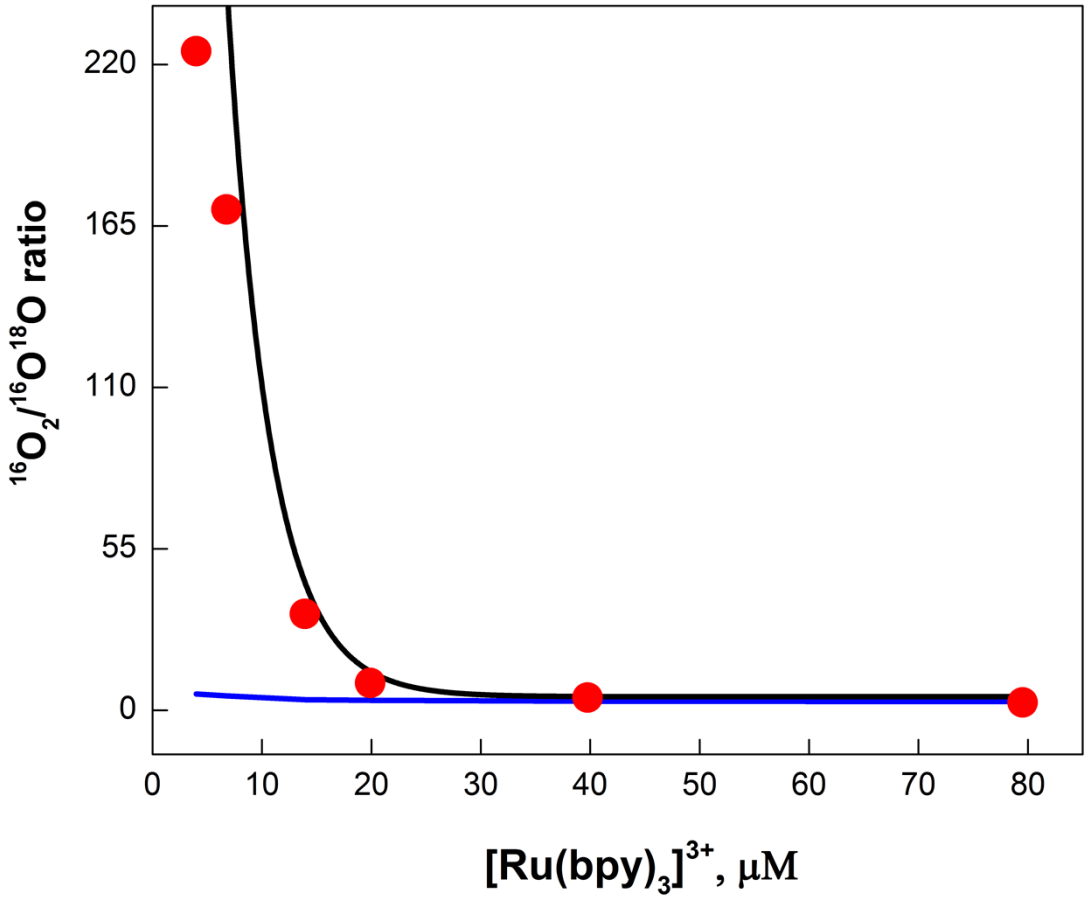

Figure S7. Independent repeat of the FTA experiment using a different source of $Co(ClO_4)_2$. **Red symbols:** isotopologue ratios of oxygen evolved after the injection of 100 µl $H_2{}^{18}O$ (90%) containing various $[Ru(bpy)_3]^{3+}$ concentrations to preformed Co/M2P-oxide NP having ^{16}O-labelled bridges and terminal ligands. The final $H_2{}^{18}O$ enrichment was 15%. The Co/M2P-oxide NP's were formed by the injection of 10 µl $[Ru(bpy)_3]^{3+}$ dissolved in natural abundance water into reaction mixtures (600 µl) containing 10 µM $Co(ClO_4)_2$, 14 µM M2P and 20 mM P_i (pH 7). The final $[Ru(bpy)_3]^{3+}$ concentration was 76 µM. **Lines:** Best fits of the $^{16}O_2/^{16}O^{18}O$ (circles) ratios using equations 2+3 (blue BWNA, Co/[cat] = 1.4 µM and n_i = 4) and equations 4+5 (black line; IMOC, Co/[cat] = 2.35 and n_i = 3.5), respectively.

Text 2: Unrestricted FTA analysis

To further study both the deviations from the IMOC model at low $[Ru(bpy)_3]^{3+}$ concentrations and the possible effects of the implicit assumptions, we analyzed the data also in a less restrictive way. In this approach, we fitted the experimental isotopologue ratios with freely variable fractions of possible isotopologue distributions of molecular oxygen. For this we considered in addition to the isotopologue compositions for the first and the subsequent turnovers (see above) also the possibility of an injection artifact caused by O_2 that is formed in the syringe containing 90% $H_2{}^{18}O$ and $[Ru(bpy)_3]^{3+}$. This was done because we noticed that blank injections contained a small incubation time dependent amount of $^{18}O_2$ (see SI Figure S5 and ref[2]). For BWNA this results in:

$$\begin{bmatrix} {}^{16}O_2 \\ {}^{16,18}O_2 \\ {}^{18}O_2 \end{bmatrix}_{total} = \begin{bmatrix} 0.8483 \\ 0.1514 \\ 0.0003 \end{bmatrix} \times a + \begin{bmatrix} 0.7225 \\ 0.2550 \\ 0.0225 \end{bmatrix} \times b + \begin{bmatrix} 0.0100 \\ 0.1800 \\ 0.8100 \end{bmatrix} \times c \qquad \text{Eq. S1}$$

while for intramolecular coupling it follows:

$$\begin{bmatrix} {}^{16}O_2 \\ {}^{16,18}O_2 \\ {}^{18}O_2 \end{bmatrix}_{total} = \begin{bmatrix} 0.99600 \\ 0.00399 \\ 0.000004 \end{bmatrix} \times a + \begin{bmatrix} 0.7225 \\ 0.2550 \\ 0.0225 \end{bmatrix} \times b + \begin{bmatrix} 0.0100 \\ 0.1800 \\ 0.8100 \end{bmatrix} \times c \qquad Eq.\,S2$$

The free parameters *a*, *b*, *c* represent the fractions of each type of isotopologue distribution, and these fractions were forced to add up to 1. No negative values were allowed, except for the injection artifact (*c*), which owing to its reaction time dependence could be slightly larger or smaller than the value determined in the blank injections containing the respective amount of $[Ru(bpy)_3]^{3+}$. In this approach the pairs of O_2 isotopologue ratios were fitted separately for each $[Ru(bpy)_3]^{3+}$ concentration (Table S1).

The fit results displayed in Table S1 demonstrate that the discrepancy observed for 7.6 µM $[Ru(bpy)_3]^{3+}$ in the IMOC (Table 1; Eq. 4 and 5) can be explained with less than 2 % of double turnovers (plus an even smaller correction for the injection). By contrast, also with this flexible fit approach no acceptable fit was found for the BWNA mechanism. Thus, BWNA can be ruled out to be the dominant pathway for O–O bound formation during water-oxidation catalyzed by Co/M2P-oxide NP.

Table S1. *Fractions of O_2 isotopologue distributions for IMOC and BWNA.*[a]

$[Ru(bpy)_3]^{3+}$, µM	IMOC				BWNA			
	Fractions of O_2			diff [2]	Fractions of O_2			diff [2]
	a	b	c		a	b	c	
7.6	0.983	0.017	3.6×10^{-4}	1.1×10^{-6}	0.998	0.000	2.1×10^{-3}	12636
11.4	0.918	0.081	1.9×10^{-4}	1.0×10^{-12}	0.985	0.000	1.0×10^{-2}	1169
13.3	0.825	0.175	2.0×10^{-5}	1.9×10^{-13}	0.985	0.000	1.5×10^{-2}	204
15.2	0.711	0.288	4.1×10^{-4}	2.2×10^{-14}	0.984	0.000	1.5×10^{-2}	42
19	0.613	0.386	6.1×10^{-5}	8.2×10^{-16}	0.983	0.000	1.5×10^{-2}	11
38	0.339	0.659	7.2×10^{-4}	2.4×10^{-17}	0.813	0.173	1.2×10^{-2}	1.3×10^{-15}
76	0.339	0.659	7.2×10^{-4}	9.3×10^{-17}	0.813	0.173	5.8×10^{-3}	1.9×10^{-15}

[a] *The values were derived from individual best fits of equations S1 and S2, respectively, to the experimental isotopologue ratios obtained for each $[Ru(bpy)_3]^{3+}$ concentration. Diff² is the sum of the squared differences between the experimental and calculated $^{16}O_2/^{16,18}O_2$ and $^{16,18}O_2/^{18}O_2$ isotopologue ratios at each $[Ru(bpy)_3]^{3+}$concentration.*

Mixture of intramolecular coupling with bulk water nucleophilic attack for the first turnover

$$\begin{bmatrix} ^{16}O_2 \\ ^{16,18}O_2 \\ ^{18}O_2 \end{bmatrix}_{total} = \begin{bmatrix} 0.99600 \\ 0.00399 \\ 0.000004 \end{bmatrix} \times a + \begin{bmatrix} 0.8483 \\ 0.1514 \\ 0.0003 \end{bmatrix} \times b + \begin{bmatrix} 0.0100 \\ 0.1800 \\ 0.8100 \end{bmatrix} \times c \qquad Eq.S3$$

The free parameters *a*, *b*, *c* are identical to those that explained above. In this approach the pairs of O_2 isotopologue ratios were fitted separately for 7.6 µM $[Ru(bpy)_3]^{3+}$ concentration (Table S2).

The fit results displayed in Table S2 demonstrate that the O_2 isotopologue ratio obtained for this lowest concentration of $[Ru(bpy)_3]^{3+}$ can be equally well be explained by only IMOC plus less than 2 % of double turnovers (plus an even smaller correction for the injection), and by a mixture of 97% IMOC and 3% BWNA (plus a minor correction for the injection). Thus, IMOC is in any case by far the dominant pathway for O–O bound formation during water-oxidation catalyzed by Co/M2P-oxide NP.

Table S2 *Comparison of IMOC (plus double turnover) and a hybrid IMOC + BWNA mechanism as explanation for the oxygen isotopologue ratio induced by 7.6 µM $[Ru(bpy)_3]^{3+}$.*[a]

	$^{16}O_2/^{16,18}O_2$	$^{16,18}O_2/^{18}O_2$	Fractions of O_2			diff [2]
			a	b	c	
experimental	118 ± 10	76 ± 10	-	-	-	-
IMOC + BWNA (Eq. 3)	117.2	74.8	0.97	0.03	0.0001	1.9
IMOC (Eq. S2)	118.0	76.0	0.983	0.017	0.0004	1.1×10^{-6}

[a] *The values were derived from best fits of equations S2 and S3, respectively, to the experimental isotopologue ratios obtained for 7.6 µM $[Ru(bpy)_3]^{3+}$. Diff² is the sum of the squared differences between the experimental and calculated $^{16}O_2/^{16,18}O_2$ and $^{16,18}O_2/^{18}O_2$ isotopologue ratios.*

Supplemental References

1 M. Risch, D. Shevchenko, M. F. Anderlund, S. Styring, J. Heidkamp, K. M. Lange, A. Thapper and I. Zaharieva, *Int. J. Hydrogen Energy*, 2012, **37**, 8878-8888.

2 P. K. Ghosh, B. S. Brunschwig, M. Chou, C. Creutz and N. Sutin, *J. Am. Chem. Soc.*, 1984, **106**, 4772-4783.

3 Z. Q. Huang, Z. Luo, Y. V. Geletii, J. W. Vickers, Q. S. Yin, D. Wu, Y. Hou, Y. Ding, J. Song, D. G. Musaev, C. L. Hill and T. Q. Lian, *J. Am. Chem. Soc.*, 2011, **133**, 2068-2071.

4 R. D. Gerardi, N. W. Barnett and P. Jones, *Analytica Chimica Acta*, 1999, **388**, 1-10.